Time Schemes for Strongly Nonlinear Damping Equations

EUGENIA KALNAY AND MASAO KANAMITSU*

Development Division, National Meteorological Center, Washington, DC

(Manuscript received 24 September 1987, in final form 10 March 1988)

ABSTRACT

In atmospheric models that include vertical diffusion and surface fluxes of heat and moisture it is common to observe large amplitude "fibrillations" associated with these nonlinear damping terms. In this paper this phenomenon is studied through the analysis of a simple nonlinear damping equation, $\partial X/\partial t = -(KX^P)X + S$. It is concluded that the behavior of several time schemes for the strongly nonlinear damping equations currently used can be quite pathological, with either large amplitude oscillations, or even nonoscillatory but incorrect solutions. Also presented are new simple schemes, which are easy to implement and have a much wider range of stability. These schemes are applied in the new National Meteorological Center (NMC) spectral model.

1. Introduction

An equation of the form

$$C\frac{\partial X}{\partial t} = -E(X - X_a) + R \qquad (1.1)$$

is widely used in atmospheric models to forecast ground temperature. The left side of (1.1) represents the change in time of heat storage of the ground top layer, with heat capacity C and temperature X. The first term on the rhs represents the transfer of both sensible and latent heat from ground to air, and is proportional to the difference between the ground temperature and the air temperature X_a. The R includes other heat fluxes such as those due to solar and longwave radiation, and the transfer of heat between the top ground layer and other sublayers.

The exchange coefficient E usually depends on the static stability of the atmospheric surface layer. For statically stable layers, where $X - X_a < 0$, E is quite small, but it increases to large values for neutral or unstable surface layers, for which $X - X_a \geq 0$. In addition, since the first term on the rhs of (1.1) also represents the effects of latent heat flux, E also includes the dependence of the saturation vapor pressure on the temperature. This can become very large when evaporation dominates the surface flux of energy (see Appendix).

For thin ground layers, the use of an explicit time scheme to integrate (1.1) would require excessively small time steps. For this reason, most atmospheric models attempt to use at least partially implicit time schemes for this equation. However, in most parameterizations the exchange coefficient is a very nonlinear function of the stability as well as of the surface wind, and, as mentioned before, there is a nonlinearity associated with the dependence of the saturation specific humidity on temperature. These nonlinearities make the use of a fully implicit time scheme impractical.

The National Meteorological Center (NMC) model uses a typical *partially* implicit scheme. At each time step t_n, the exchange coefficient is computed in terms of the current air and soil temperature. This value, E_n, is then used in (1.1) to update X_{n+1} using an implicit backward scheme. Although this scheme is generally satisfactory, for strongly heated surface layers or very wet land areas it can lead to spurious oscillations. Figure 1a is an example of such an oscillation in the NMC model during a one day integration, as observed in a Gaussian grid point located at 10°S, 60°W. The top ground temperature during the hours of strong sunshine and evaporation has a two-time step oscillation with an amplitude of more than 2°K. The air surface temperature (not shown) also oscillates, but with an amplitude of only 0.2°K, and the oscillation observed in the temperature of the subsoil layer is even smaller. This suggests that this oscillation originates in the top ground layer, and is due to the use of the combined explicit coefficient/implicit temperature scheme described above. Although the ground temperature oscillates about a mean value which is not unreasonable for such a location, during the oscillations high surface temperature values X_{n+1} are multiplied by low (stable) exchange coefficients E_n, and vice versa. As a result,

* On leave from the Japan Meteorological Agency.

Corresponding author address: Eugenia Kalnay, Chief, Development Division, NOAA/National Weather Service, National Meteorological Center, Washington, D.C. 20233.

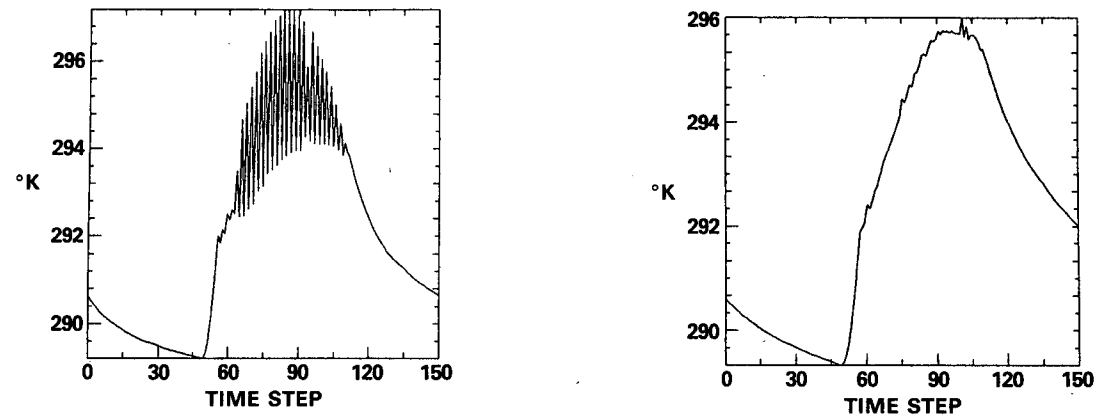

FIG. 1. (a) Top soil temperature at a point located at 10°S, 60°W (SW Brazil) using the NMC Dynamical Extended Range Prediction (DERF) model with rhomboidal truncation of 40 waves (R40) and the explicit coefficient/implicit temperature time scheme. The integration with a time step of 576 sec corresponds to 24 h starting on 0000 UTC 21 January 1985. (b) As in (a), but with scheme h used for the surface temperature equation (section 2).

the oscillation results in smaller than expected surface-to-air heat and moisture fluxes and little convective rain at that point.

The tendency of the atmospheric variables due to vertical diffusion is another example of a strongly nonlinear damping equation used in atmospheric models. For example,

$$\frac{\partial X_a}{\partial t} = \frac{\partial}{\partial z} \nu \frac{\partial X_a}{\partial z} \tag{1.2}$$

is a typical formulation of the vertical diffusion of atmospheric temperatures, where the vertical diffusion coefficient ν depends on atmospheric stability and, as such, is a strongly nonlinear function of X_a. A scheme using an explicit coefficient ν_n computed at time step t_n, and an implicit backward scheme for X_{an+1}, similar to the explicit/implicit scheme described above for the surface temperature equation, has been in use both at NMC and at the European Centre for Medium-range Weather Forecasts (ECMWF). Two time step oscillations have been reported at both centers (P. Long, personal communication; Jarraud et al. 1985).

In this paper we analyze a simple nonlinear damping equation

$$\frac{\partial X}{\partial t} = -(KX^P)X + S \tag{1.3}$$

and test several time schemes both for accuracy and stability. Here X is the temperature difference between ground and air, the factor (KX^P) represents the exchange coefficient, with K constant, and all slowly varying processes are included in S.[1] We conclude that the behavior of several time schemes for the strongly nonlinear equation currently in use can be quite pathological, with either large amplitude oscillations or even nonoscillatory but incorrect solutions. We also present new simple schemes which are easy to implement and have a much wider range of stability. Figure 1b represents the same example as Fig. 1a, but using one of these schemes (scheme h).

Section 2 contains a description of a number of time schemes that have been considered for nonlinear damping equations. In section 3, a linear stability analysis of these schemes is performed, and in section 4 examples of numerical integrations of the nonlinear equation are presented. In section 5, experiments performed implementing several schemes on the NMC model are discussed, and section 6 contains a summary and recommendations.

2. Time schemes

In this section we will only consider two time-level schemes. Three time-level schemes have computational modes which in the case of centered schemes (leapfrog) are absolutely unstable. Except for schemes *b* and *c*, which are absolutely stable, these two time-level schemes are conditionally stable.

a. Forward explicit

$$\frac{X_{n+1} - X_n}{\Delta t} = -KX_n{}^P X_n + S.$$

This is the simplest scheme to implement, but, as will be shown, it is also the scheme with the smallest range of stability.

b. Backward implicit

$$\frac{X_{n+1} - X_n}{\Delta t} = -KX_{n+1}^P X_{n+1} + S.$$

[1] We assume $X \geq 0$. If $X < 0$, the exchange coefficient should be $K|X|^P$.

In practice, this absolutely stable scheme is difficult to implement except using iterative methods.

c. Centered implicit (Crank–Nicholson)

$$\frac{X_{n+1} - X_n}{\Delta t} = -K\left(\frac{X_n + X_{n+1}}{2}\right)^P \frac{X_n + X_{n+1}}{2} + S.$$

This is the only scheme with second order time truncation errors. It combines absolute stability with higher accuracy, but it is also the most difficult to implement.

d. Explicit coefficient, implicit temperature

$$\frac{X_{n+1} - X_n}{\Delta t} = -KX_n{}^P X_{n+1} + S.$$

This scheme, which is easy to implement, is similar to the ones used at NMC and at many other centers.

Although this scheme is more stable than the explicit scheme, it still suffers from oscillations for large values of X and P, as discussed in the Introduction. We therefore consider the following alternative schemes that might alleviate the problem.

e. Predictor–corrector coefficient (t_*), implicit temperature

$$\frac{X_* - X_n}{\Delta t} = -KX_n{}^P X_* + S,$$

$$\frac{X_{n+1} - X_n}{\Delta t} = -KX_*^P X_{n+1} + S.$$

This scheme is easy to implement but requires two computations of the tendency.

f. Averaged coefficient (t_*, t_n), implicit temperature

$$\frac{X_* - X_n}{\Delta t} = -KX_n{}^P X_* + S,$$

$$\frac{X_{n+1} - X_n}{\Delta t} = -K\left(\frac{X_n{}^P + X_*^P}{2}\right)X_{n+1} + S.$$

This scheme has been implemented in the computation of the vertical diffusion terms of the model used for the Dynamical Extended Range Forecast (DERF) experiment performed at NMC in 1986–87. As scheme e, it requires two computations of the tendency.

g. Explicit coefficient, extrapolated temperature

$$\frac{X_{n+1} - X_n}{\Delta t} = -KX_n{}^P[\gamma X_{n+1} + (1 - \gamma)X_n] + S.$$

This scheme has been proposed and implemented at ECMWF (Jarraud et al. 1985) in order to avoid two time step oscillations in the vertical diffusion equation (1.2). It is clear that with $\gamma = 0$, this scheme coincides with scheme a, where with $\gamma = 1$, it becomes the same as scheme *d*. At ECMWF the extrapolated scheme is used with the value $\gamma = 1.5$.

h. Explicit coefficient, implicit temperature, followed by time filter

$$\frac{X_* - X_n}{\Delta t} = -KX_n{}^P X_* + S,$$

$$X_{n+1} = (1 - A)X_* + AX_n.$$

This scheme requires only minimal modification of scheme *d*, and is very easy to implement. However, the fact that the time filter is centered at time $t_n + A\Delta t$, and not at t_{n+1}, suggests that it is not consistent with the continuous equations. The results of sections 3 and 4 indicate that a modification of this scheme, in which the time filter with $A = 0.5$ is only invoked when the exchange coefficient becomes large, is an optimal choice.

i. Double time step, explicit coefficient, implicit temperature, followed by time average

$$\frac{X_* - X_n}{2\Delta t} = -KX_n{}^P X_* + S,$$

$$X_{n+1} = (X_* + X_n)/2.$$

This scheme is consistent, easy to implement, and highly damping of two time step oscillations. However, as will be shown, it is somewhat less stable than scheme *h* with $A = 0.5$. Although it is computed as a time average of an estimate of X corresponding to time t_{n+2} and the value of X at time t_n, it can be shown that it also corresponds to the extrapolated scheme g, with $\gamma = 2$.

One of the reviewers (M. Jarraud, personal communication) has pointed out that all of the scheme with explicit exchange coefficient $C_n = KX_n{}^P$ can be expressed as

$$\frac{X_{n+1} - X_n}{\Delta t} = \beta[-C_n X_n + S]$$

where β is a function of C_n. Then, for scheme *a*, $\beta_a = 1$; for scheme *d*, $\beta_d = 1/(1 + C_n\Delta t)$; for scheme *g*, $\beta_g = 1/(1 + C_n\Delta t\gamma)$; for scheme *h*, $\beta_h = (1 - A)/(1 + C_n\Delta t)$; and for scheme *i*, $\beta_i = 1/(1 + 2C_n\Delta t)$.

j. Linear approximation of the implicit backward scheme b

Jarraud (personal communication) has also indicated the existence of a scheme (Bidet et al. 1979) which for Eq. (1.1) is of the form

$$C\frac{X_{n+1}-X_n}{\Delta t} = -E_n(X_n - X_a) + \frac{\partial}{\partial X}[E_n(X - X_a)]_n(X_{n+1} - X_n),$$

i.e., a linear approximation of the implicit backward scheme *b*, where the derivative on the right-hand side is computed at every time step. For the simple Eq. (1.3) it becomes

$$\frac{X_{n+1}-X_n}{\Delta t} = -K[X_n{}^{P+1} + (P+1)X_n{}^P(X_{n+1} - X_n)] + S$$
$$= -KX_n{}^P[(P+1)X_{n+1} - PX_n] + S,$$

i.e., it is of the extrapolated type with $\gamma = P + 1$. The scheme has the same linear amplification factor as the backward implicit scheme *b*, and therefore it is absolutely stable. This is an excellent scheme, with only two possible drawbacks. The first is that the computation of the derivative of the flux term $E(X)(X - X_a)$ with respect to the temperature X may not be easily computed, especially if it is not given in an analytical form. The second is that for very nonlinear terms, this scheme results in a strong extrapolation, and therefore larger truncation errors (see section 4).

3. Linear stability analysis

If we assume that the temperature X is close to the equilibrium solution X_0,

$$X = X_0 + \delta X, \tag{3.1}$$

where $X_0{}^{P+1} = S/K$, and replace (3.1) and (1.3) retaining only terms linear in δX, we obtain

$$\frac{\partial \delta X}{\partial t} = -KX_0{}^P(P\delta X + \delta X). \tag{3.2}$$

Here the first term in parentheses corresponds to the exchange coefficient KX^P factor, and the second to the temperature X.

A linear stability analysis can now be easily performed. For example, for the explicit coefficient/implicit temperature scheme *d* of section 2, the corresponding linearized scheme is

$$\delta X_{n+1} = \delta X_n - \alpha(P\delta X_n + \delta X_{n+1}) \tag{3.3}$$

where $\alpha = KX_0{}^P\Delta t$ is a positive nondimensional numerical stability parameter proportional to the equilibrium exchange coefficient $KX_0{}^P$ and to the time step Δt. We can now determine the amplification factor:

$$\rho = \frac{\delta X_{n+1}}{\delta X_n} = \frac{1 - \alpha P}{1 + \alpha}. \tag{3.4}$$

TABLE 1. Amplification factor and linear stability criterion for nine time schemes applied to the linearized damping equation (3.2). Schemes *e* and *f* become unstable without oscillatory behavior. Schemes *a*, *d* and *i* can be derived from scheme *g* with $\gamma = 0$, 1 and 2 respectively.

Scheme	Amplification factor ρ	Linear stability criterion
a. Forward explicit	$1 - \alpha(P+1)$	$\alpha(P+1) < 2$
b. Backward implicit	$1/(1 + \alpha(P+1))$	Absolutely stable
c. Centered implicit (Crank–Nicholson)	$\frac{(1 - \alpha(P+1)/2)}{(1 + \alpha(P+1)/2)}$	Absolutely stable
d. Explicit coefficient, implicit temperature	$(1 - \alpha P)/(1 + \alpha)$	$\alpha(P-1) < 2$
e. Predictor-corrector coefficient (t_*), implicit temperature	$\frac{1 - \alpha(P-1) + (\alpha P)^2}{(1+\alpha)^2}$	$\alpha(P^2 - 2) < P + 1$
f. Average coefficient (t_n, t_*), implicit temperature	$\frac{1 - \alpha(P-1)\frac{\alpha^2 P}{2} + \frac{(\alpha P)^2}{2}}{(1+\alpha)^2}$	$\alpha(P-2) < 2$
g. Explicit coefficient, extrapolated temperature	$\frac{1 - \alpha(P+1-\gamma)}{1 + \alpha\gamma}$	$\alpha(P+1-2\gamma) < 2$ For $\gamma = 1.5$, it reduces to $\alpha(P-2) < 2$
h. Explicit coefficient, implicit temperature with time filter	$(1-A)\left(\frac{1-\alpha P}{1+\alpha}\right) + A$	$\alpha(P(1-A) - 1 - A) < 2$ For $A = 0.5$ it reduces to $\alpha(P-3) < 4$
i. Double time step, explicit coefficient, implicit temperature with time average filter	$\frac{1 - \alpha(P-1)}{1 + 2\alpha}$	$\alpha(P-3) < 2$
j. Linear approximation of backward implicit scheme b	$1/(1 + \alpha(P+1))$	Absolutely stable

The condition $|\rho| < 1$ is necessary and sufficient for stability and convergence, since then and only then will $\delta X_n \to 0$ as $n \to \infty$. However, only if $0 < \rho < 1$ will δX_n be monotonically damped. If $-1 < \rho < 0$ the linear solution will exhibit damped oscillations.

If $|\rho| > 1$, the linearized scheme is unstable, and the linear solution grows exponentially with time. However, as will be shown in section 4, when the condition for linear stability is violated, *the nonlinear time integration does not "blow up"*. Instead it exhibits an insidious behavior, with large amplitude oscillations if $\rho < -1$, or convergence to an incorrect solution if $\rho > 1$.

It is clear from Eq. (3.4) that the stability criterion for scheme *d* depends not only on the value of the stability parameter α, as is usually the case in damping equations, but also on the power P, which represents the nonlinearity of the exchange coefficient. In the case of scheme *d*, for example, ρ becomes negative, and the solution oscillates if $\alpha P > 1$. The linear scheme becomes unstable ($\rho < -1$) if $\alpha P - 1 > 1 + \alpha$, or if $\alpha(P - 1) > 2$. By contrast, the simple forward explicit scheme a becomes unstable with $\rho < -1$ when $\alpha(P + 1) > 2$.

As a second example we consider scheme *e*, in which the coefficient is obtained from a predictor step.

$$\delta X_* = \delta X_n - \alpha(P\delta X_n + \delta X_*)$$

$$\delta X_{n+1} = \delta X_n - \alpha(P\delta X_* + \delta X_{n+1}).$$

Now $\rho = [1 - \alpha(P-1) + (\alpha P)^2]/(1+\alpha)^2$ is always greater than zero, and no oscillatory behavior can take place. The linear scheme becomes unstable if $\rho > 1$, which occurs if $\alpha(P^2 - 2) > P + 1$.

Table 1 summarizes the dependence of the amplification factor ρ on α and the power P, as well as the condition for linear stability.

The neutral stability curves $|\rho| = 1$ for the different schemes are plotted on Fig. 2, with full lines for those schemes for which $\rho = -1$, corresponding to oscillatory behavior, and dashed for the nonoscillatory schemes *e* and *f*, for which $\rho = 1$ under neutral stability. It is clear that the explicit coefficient, implicit temperature scheme *d* has a much larger range of stability than the explicit scheme *a*. However, for strongly nonlinear equations, when $P > 3$, scheme *d* is unstable even for $\alpha < 1$! Schemes *e* and *f* show no oscillatory behavior, but scheme *f* has a much wider range of stability. Scheme *g*, with an extrapolated temperature, and $\gamma = 1.5$ as used at ECMWF, has a range of stability equal to that of scheme *f*, but when unstable it exhibits oscillatory rather than damped behavior. The partially explicit schemes with widest stability range are scheme *h*, with $A = 0.5$, and scheme *i*. The two implicit schemes *b* and *c* are absolutely stable.

Consistency of the finite difference schemes with the continuous equation (3.2) requires that as $\Delta t \to 0$ (i.e., as $\alpha \to 0$), $\rho \to 1 - \alpha < P + 1$) since for the exact solution $\rho = e^{-\alpha(P+1)}$. It is easy to see that this criterion is satisfied by all the schemes except scheme *h*, for which $\rho \to 1 - \alpha(P+1)/2$ as Δt or $\alpha \to 0$.

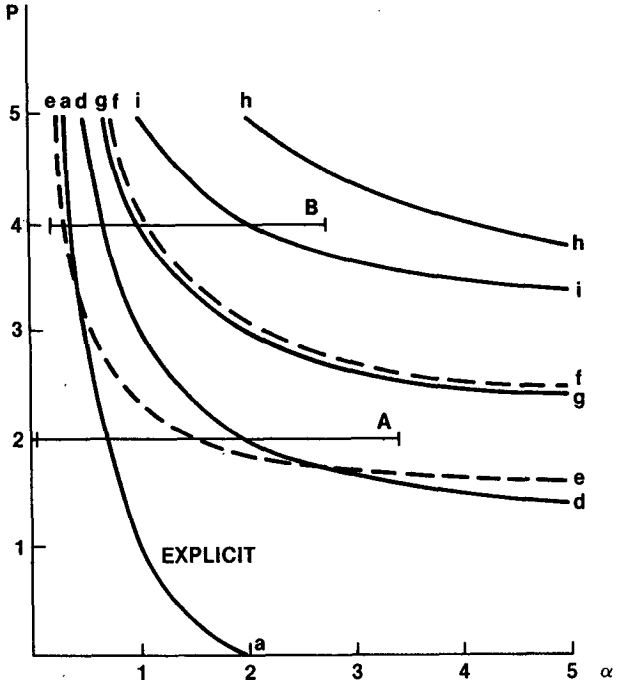

FIG. 2. Neutral stability curves corresponding to the seven partially explicit schemes of Table 1. (The two implicit schemes, *b* and *c*, are absolutely stable.) Full lines correspond to oscillatory schemes ($\rho = -1$). Dashed lines correspond to nonoscillatory schemes ($\rho = 1$). Schemes *f* and *g* have the same range of stability. The abscissa $\alpha = KX_0{}^P \cdot \Delta t = C \cdot \Delta t$ is equal to the product of the exchange coefficient and the time step. The P is the effective power of the temperature in the exchange coefficient. The horizontal lines, A and B, represent the values of P and ranges of α in the experiments A and B of section 4.

For large values of α and P, consistency cannot be maintained, since large time truncation errors are inevitable. In this case, however, we should require that the numerical scheme in use reproduce the "adjustment" that takes place in the case of the continuous equation: $\rho \to 0$, $\delta X \to 0$ and the temperature X quickly converges to its equilibrium value X_0. This condition is satisfied by all the *stable* schemes.

This consideration suggests the following modification of scheme *h* with $A = 0.5$, which is the most stable of the partially explicit schemes considered here. Scheme *d* is used except when it becomes close to the unstable regime, at which time the time filter of scheme *h* is invoked and an "adjustment" then takes place. For the numerical experiments presented in section 4 we invoked the time filter whenever $\alpha(P-1) \geq 1$. In atmospheric models, the filter can be used whenever the exchange coefficient becomes large, at which time the equilibrium solution should be quickly attained.

4. Nonlinear numerical integrations

In this section the results of two sets of numerical integrations of Eq. (1.3) with the schemes described in section 2 are presented. In both cases we have used for the driving term

$$S_n = 1 + \sin(2\pi n/20), \qquad (4.1)$$

simulating a "diurnal cycle" of 20 time steps, and we have taken $K = 10$ and $\Delta t = 1$. The first case represents a moderately nonlinear equation, with $P = 2$, and the second case corresponds to a strongly nonlinear regime, with $P = 4$. The nonlinear exchange coefficient is represented by $C = KX^P$.

Case A: $P = 2$. In this case, the linear stability parameter $\alpha = C\Delta t$ varies for the exact solution between $\alpha_{\min} = 0.03$ and $\alpha_{\max} = 3.41$ during the course of the integration. Figure 2 indicates that for this case only schemes *a* (explicit: C_nX_n), the basic scheme *d* (explicit/implicit: C_nX_{n+1}), and scheme *e* (predictor-corrector/implicit: C_*X_{n+1}) are linearly unstable during part of the cycle.

Figure 3 presents with full lines the result of numerical integrations with nine time schemes for 50 time steps each. With each integration, for comparison, we also show in broken lines the results corresponding to the Crank–Nicholson scheme *c*, $[(C_n + C_{n+1})/2 \cdot (X_n + X_{n+1})/2]$ which, being centered in time, is the only scheme with second-order truncation errors, and therefore is the most accurate of the schemes considered here.

The first panel on the top row compares the centered implicit scheme *c* and the backward implicit scheme *b* ($C_{n+1}X_{n+1}$). Both schemes are linearly absolutely stable and nonoscillatory (section 3) and their nonlinear integrations agree well except that the backward implicit scheme has a slight delay, and an underestimation of the amplitude of the minimum value of X. In the second panel, the integration with the basic scheme *d*, (C_nX_{n+1}), shows a remarkable result. *Even though the linear stability criterion is violated,* with $\rho < -1$, *the nonlinear integration is bounded, and the solution bounces between two values, one much larger and one much smaller than the correct solution.* The third panel on the top row presents the results of the scheme *g* (explicit/extrapolated: $C_n[\gamma X_{n+1} + (1 - \gamma)X_n)]$ with $\gamma = 1.5$, as used at ECMWF. For this case the scheme is stable and is in excellent agreement with the centered implicit scheme.

In the second row we present three schemes where the exchange coefficient C has been modified with the intention of making the solution less oscillatory than in the basic scheme *d*. The first panel corresponds to scheme *e* (predictor-corrector/implicit: C_*X_n), and Fig. 2 indicates that for this scheme the range of stability is no better than scheme *d*. It should be remembered, however, that when the linear stability criterion is violated, the amplification factor of scheme *e* becomes greater than one, and we therefore do not expect the solution to oscillate. In the numerical integration we observe a second remarkable result: *when the linear stability criterion is violated,* with $\rho > 1$, *the scheme remains bounded and nonoscillatory, but the solution is completely wrong.* The second panel on the middle row corresponds to scheme *f* (averaged predictor-corrector/implicit: $[(C_n + C_*)/2]\, X_{n+1}$. This scheme has a range of stability equal to that of scheme *g* (explicit/extrapolated) with $\gamma = 1.5$, but as in the previous scheme, the linear stability analysis indicates that the scheme is nonoscillatory, with $\rho > 0$. Even though for this case the scheme is stable, the results indicate that it suffers from serious truncation errors when compared with the centered scheme. The third panel of the middle row corresponds to a scheme not discussed in section 2 because it is a three-time level scheme. Here the coefficient is averaged from the values at time step n and $n - 1$:

$$\frac{C_n + C_{n-1}}{2} X_{n+1}.$$

It seems plausible that this scheme would be less oscillatory than scheme *d*. We observe that it still has oscillations but they are period $3\Delta t$ rather than $2\Delta t$, and their amplitude is smaller than in scheme *d*.

The bottom row presents three variants of time filtered schemes. In the first one, scheme *i*, a double time step is used to update X_*, which is then averaged with X_n to obtain X_{n+1}. As discussed in sections 2 and 3, this scheme is consistent and has a much wider stability range than scheme *d*, and could also be computed as the extrapolated scheme *g* with $\gamma = 2$. The results of scheme *i* are excellent, with only minimal differences with the centered implicit scheme. The second panel of the bottom row corresponds to scheme *h*: $[C_nX_*;\ X_{n+1} = (X_n + X_*)/2]$ with the time filter applied every step. As indicated in previous sections, this scheme is very stable but is not consistent, and this results in some noticeable truncation errors for the most stable (smallest) values of the solution. Finally, in the last panel of the bottom row, we applied the time filter only when the linear stability criterion indicates that scheme *d* is unstable or only marginally stable [when $\alpha(P - 1) \geq 1$]. The results in this case are in excellent agreement with the centered implicit scheme.

It is interesting to note that for schemes in a stable range, oscillatory behavior ($-1 < \rho < 0$) presents no problem because the decay "overwhelms" the oscillations, which are hardly noticeable. (See for example the initial transient phase of the Crank-Nicholson scheme in Figs. 3 and 4.)

Case B: This is the same as case A except that now $P = 4$, corresponding to a strongly nonlinear regime in the damping equation (Fig. 4). This situation represents the atmospheric regimes near neutral stability

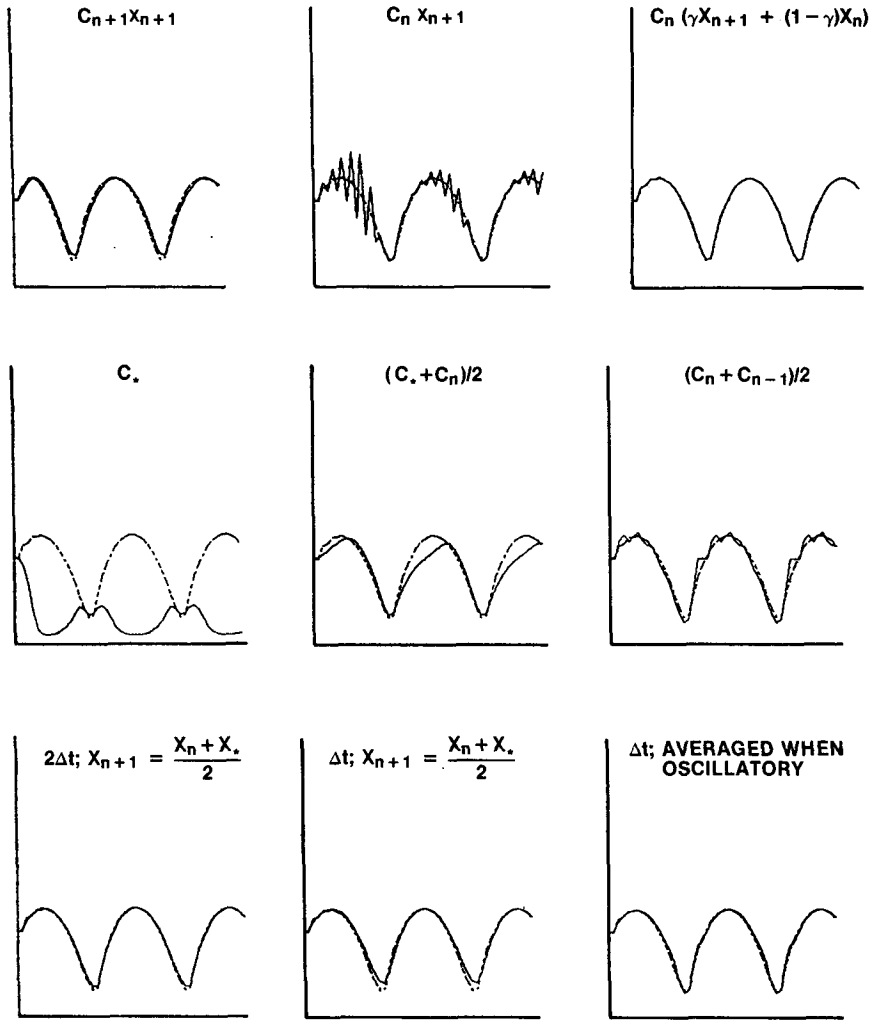

FIG. 3. Examples of numerical experiments corresponding to case A (see also Fig. 2), using ten different time schemes. The exact solution varies from 0.145 to 0.585. In each of the nine panels, the integration corresponding to scheme *c* (centered implicit) is also shown in dashed lines for comparison. The full line is the integration with the method indicated schematically on top. The time schemes are the following: Top row, left panel, scheme *b* (backward implicit); center, the basic scheme *d* (explicit coefficient, implicit temperature); right, scheme *g* (explicit coefficient, extrapolated temperature, with $\gamma = 1.5$). Middle row, left panel, scheme *e* (predictor corrector coefficient, implicit temperature); center, scheme *f* (averaged coefficient, implicit temperature); right, a 3-level scheme, with the coefficient averaged from the previous time steps, and implicit temperature. Bottom row, left panel, scheme *i* (double time step, explicit coefficient, implicit temperature, followed by time filter); center, scheme *h* (as scheme *d*, followed by time filter); right, scheme *h* but with the time filter applied only when the exchange coefficient is large.

well, when the exchange coefficient changes from very small values for statically stable conditions to large values when there is static instability. For this case, the range of the linear stability parameter $\alpha = C\Delta t = KX^P\Delta t$ varies between $\alpha_{\min} = 0.15$ and $\alpha_{\max} = 2.76$ and all schemes except *h* become at least marginally unstable (Fig. 2). The results for the basic scheme *d* (top middle panel) are similar to those of case A, except that the amplitude of the oscillations is now much larger, not unlike those observed in the NMC model (Fig. 1a). The extrapolated scheme *g* (top right panel), as could be expected from the linear stability analysis, now shows oscillations of smaller amplitude than scheme *d*. Both schemes *e* and *f*, in which the exchange coefficient is updated with a predictor–corrector scheme, are now linearly unstable, with amplification factors $\rho > 1$. This results in the absence of oscillations, but the schemes converge to a wrong value which is similar to the low value of the oscillations in scheme *d*. As a result, the nonoscillatory solution shows minima in *X* when the true solution should have maxima. The scheme with the exchange coefficient *C* averaged

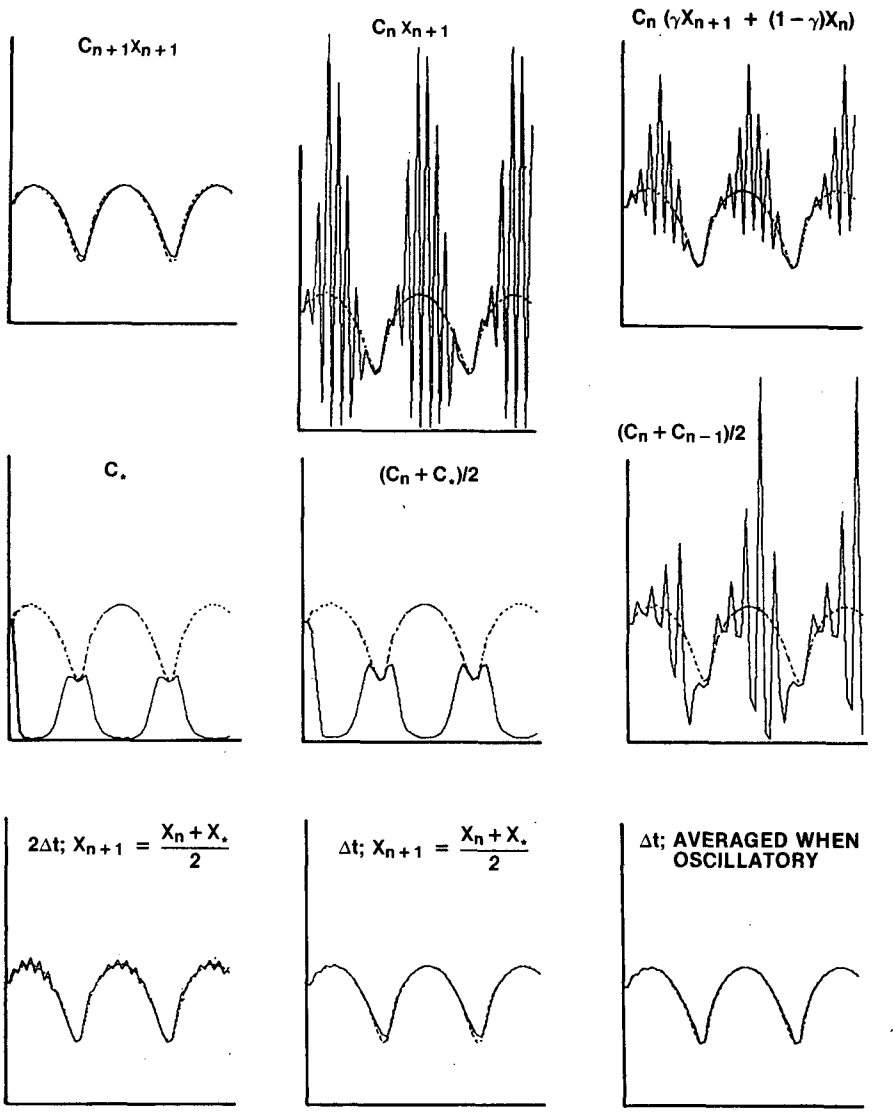

FIG. 4. As in Fig. 3, but for case B. The exact solution varies from 0.324 to 0.725.

from steps n and $n-1$ (middle right panel) has $3\Delta t$ oscillations with an amplitude comparable to scheme *d*.

In the bottom row, the scheme *i*, with the $2\Delta t$ solution averaged with the X_n solution has small amplitude oscillations, and is identical to the extrapolated scheme *g* with $\gamma = 2$ (not shown). The time filtered scheme *h*, in which the filter is applied every time step, is stable but once again shows some underestimation of the amplitude of the solution for the most stable (smallest X) range. However this same scheme, with the time filter applied only when the original scheme *d* becomes close to linear instability [$\alpha(P-1) > 1$], gives excellent results, being almost indistinguishable from the centered implicit scheme.

The scheme of Bidet et al. (1979), discussed at the end of section 2, was also tested for this case, for which $\gamma = P + 1 = 5$. It showed no oscillatory behavior but much larger errors than scheme *h*, even in the stable range.

5. Experiments with the NMC global spectral model

Some of the schemes examined in the previous sections have been tested in the fully nonlinear spectral model with full physical processes. The model is a version of the operationally used spectral model (Sela 1988). It has 18 levels in the vertical and a rhomboidal 30 (R30) wave truncation (whereas the operational model had R40 resolution) in the horizontal. Relevant to the idealized experiments performed earlier, the model incorporates diurnal variation of the incoming shortwave radiation, and the prediction of surface and soil temperatures. The model also has vertical diffusion processes in which the vertical diffusion coefficients are dependent on the static stability and the vertical wind shear. The difference equations used in the ver-

tical diffusion processes can be cast into the simple form, Eq. (1.3), if we assume that the dependent variables at adjacent levels do not vary. A control run was made using the explicit coefficient/implicit temperature scheme *d*, which is also used operationally, for both vertical diffusion and surface processes.

Examination of the time variations of various parameters for every time step at various locations on land revealed that oscillations apparently related to computational instability are caused by the vertical diffusion, surface processes, and a combination of both. Since vertical diffusion uses $2\Delta t$ instead of Δt for the time integration, the oscillations resulting from the vertical diffusion are characterized by their period of $4\Delta t$ rather than $2\Delta t$.

Figure 5a from the control (scheme *d*) run is an example of the oscillations caused solely by the vertical diffusion processes. In this case, the surface layer is statically stable and no oscillations are observed in the surface temperature. Figures 5b and 5c are the results of applying the averaged predictor–corrector coefficient/implicit temperature scheme (scheme *f*) and the double time step, explicit coefficient, implicit temperature with time average scheme (scheme *i*), both for the vertical diffusion terms. It appears that both methods are effective in removing oscillations. There seems to be a slight difference in solutions, (note the small difference of scale in the ordinate for scheme *i*) with the control and scheme *f* closer than the scheme *i*, and scheme *f* slightly smoother than scheme *i* as could be expected from the fact that for scheme *f*, the amplification factor is never negative. Note that no apparent convergence to a wrong solution is observed for the scheme *f*. This may indicate that this experiment is still within the stable range of scheme *f*, or that the Eq. (1.3) is too simple to be applied to the vertical diffusion processes.

Although in this case scheme *f* seems to be comparable to scheme *i*, it should be noted that the scheme f is nearly twice as expensive since it requires a double sweep for the entire diffusion processes.

The test of the schemes for the case of statically unstable surface layer is more dramatic. Figure 6 is the time sequence of surface temperature (a), atmospheric temperature at the lowest sigma level (b), drag coefficient (c), and local time change of surface temperature (d) for the control case (scheme *d*).

The steep increase of the drag coefficient at time step 30 is an indication of the transition from stable to unstable surface layer. This rapid transition corresponds to a high power *P* in Eq. (1.3) (see Appendix for further discussion). Large oscillations in all the variables shown here are observed when the drag coefficient exceeds about 1.5×10^{-2}. Note that the amplitude of the lowest sigma temperature is very large (about 7°C compared to 0.2°C in the previous example). Close examination of Fig. 6 reveals that the oscillations have a period of $4\Delta t$, indicating strong interaction between the surface processes and the vertical diffusion.

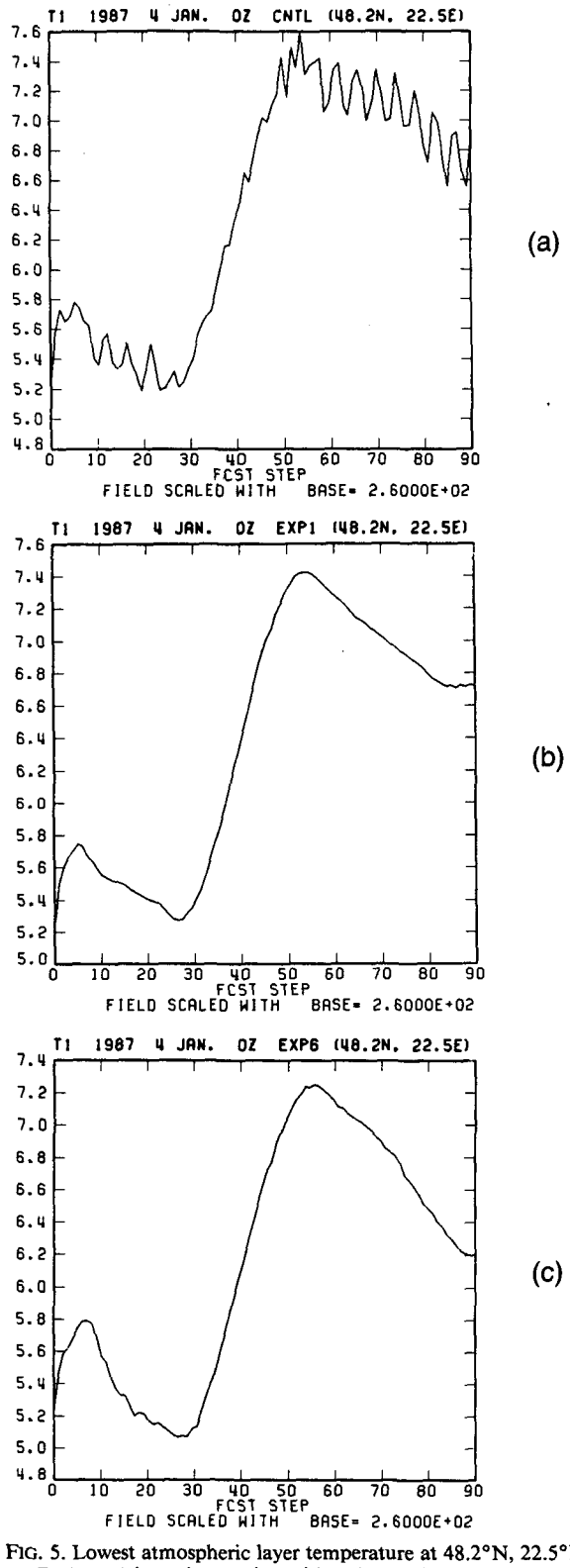

FIG. 5. Lowest atmospheric layer temperature at 48.2°N, 22.5°E (near Budapest) in an integration with a rhomboidal 30 wave truncation model showing an oscillation associated with the vertical diffusion term. The time trace corresponds to 18 h of integration with a time step of 720 sec. (a) Control run, with scheme *d* used for the vertical diffusion terms. (b) As in (a), but with scheme *f*. (c) As in (a) but with scheme *i*.

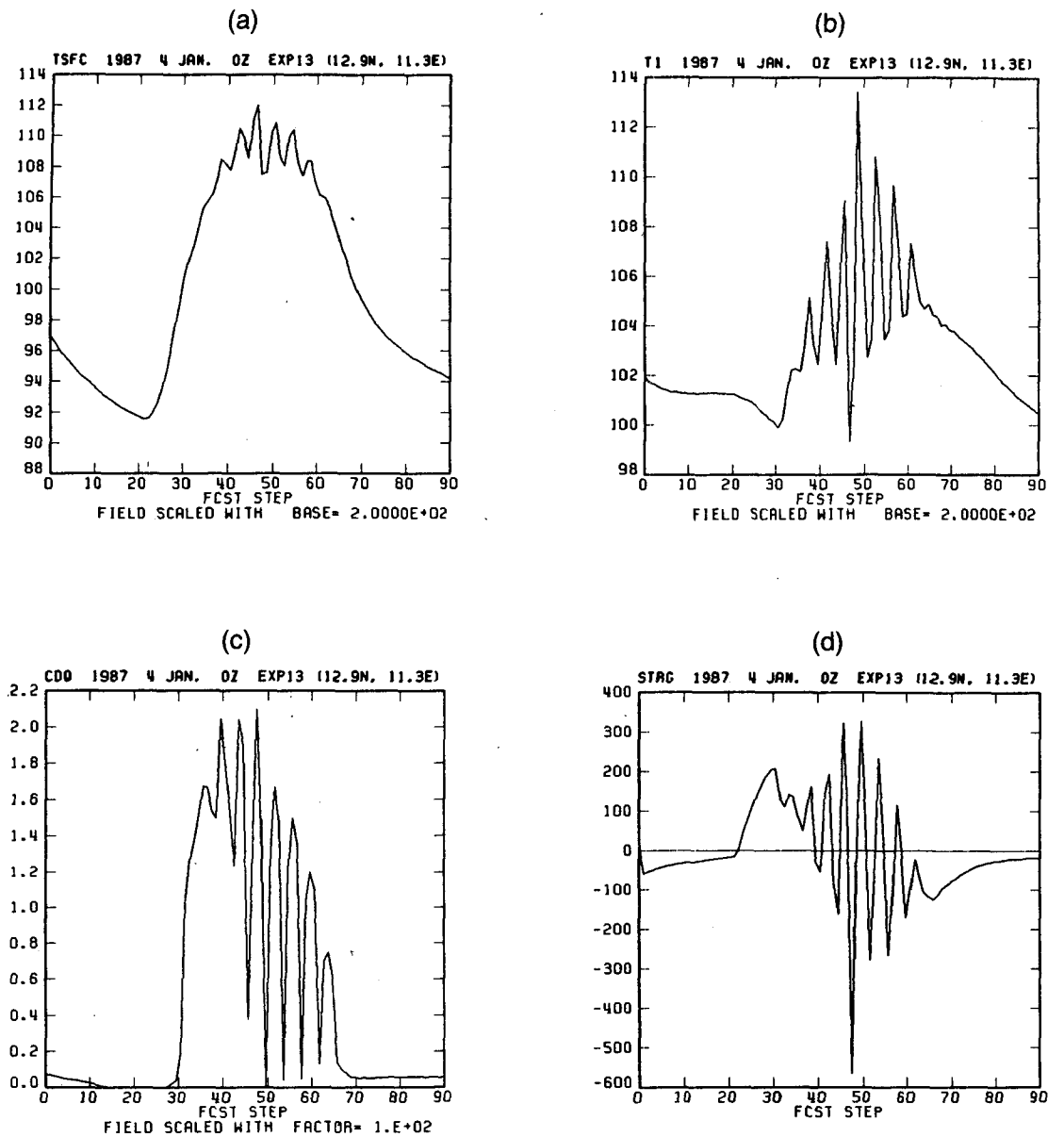

FIG. 6. Example of oscillations in the control run with scheme *d* associated with the surface temperature equation at a point located at 12.9°N, 11.3°E (near Lake Chad). (a) Top soil temperature, (b) lowest atmospheric layer temperature, (c) drag coefficient, (d) storage term (time derivative) for the top soil layer.

For this case, two additional experiments are presented. In the first one, scheme *i* (double time step, explicit coefficient/implicit temperature with a time average filter) is applied to both surface processes and vertical diffusion terms (Fig. 7). In the second, scheme *i* is applied to the vertical diffusion but scheme *h* (explicit coefficient/implicit temperature with the time filtering applied for adjustment when the surface layer is unstable) is used for the surface processes (Fig. 8). From those figures, it is clear that both schemes are very effective in removing oscillations. Because of the inconsistencies of scheme *h*, some difference in phases and peak values are observed but they are not significant.

The examples shown above do not necessarily indicate that the computational oscillations are completely eliminated by the schemes tested here. We found that the use of very large surface roughness over the tropics ($Z_0 > 200$ cm in regions of tropical forest), together with relatively low horizontal resolution that allows the use of longer time steps, can still lead to numerical oscillation, which are not completely controlled by these time schemes.

In the new global spectral model at NMC, with tri-

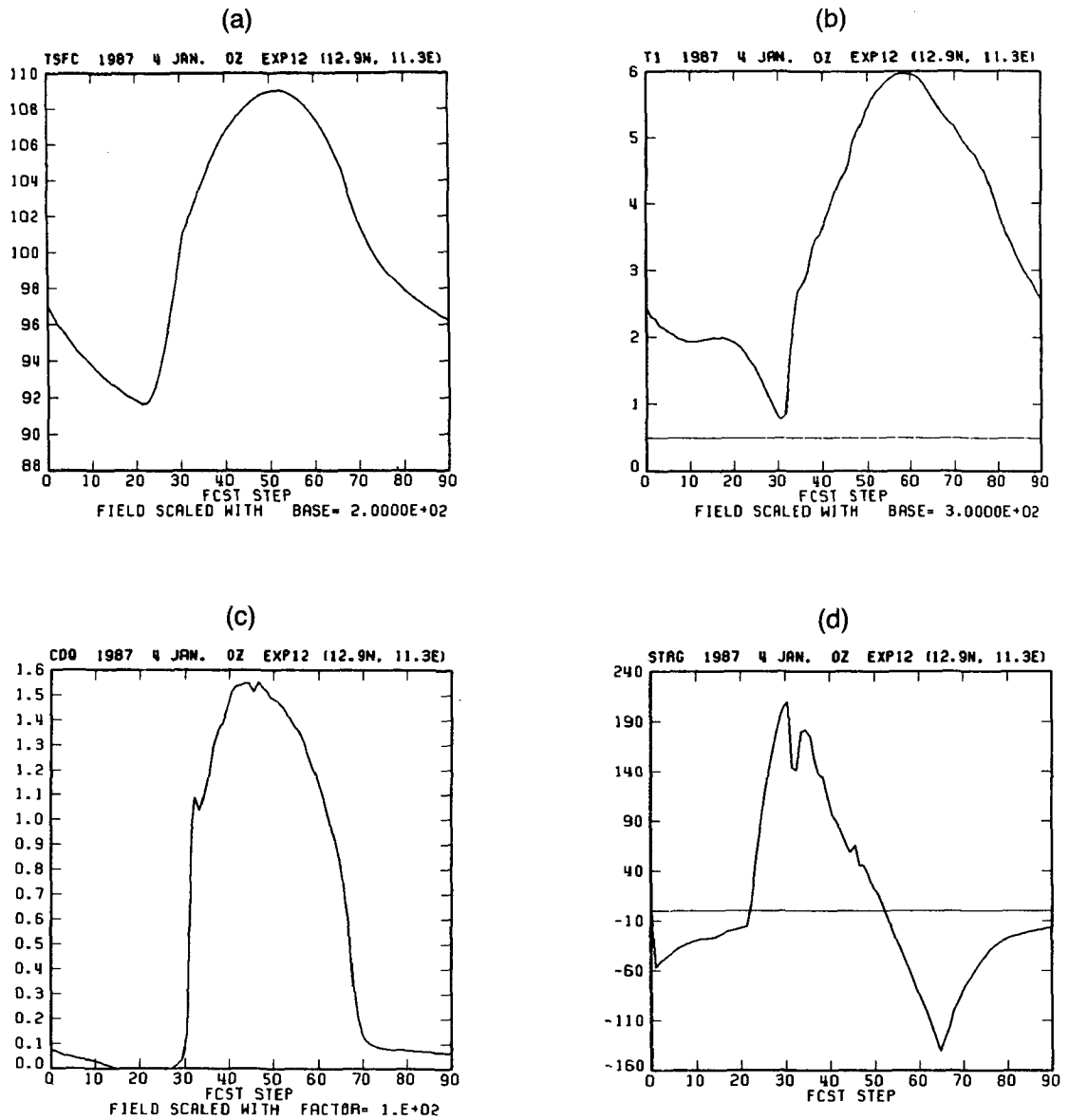

FIG. 7. As in Fig. 6 but using scheme *i* (double time step scheme *d* followed by a time filter) for both the surface temperature and the vertical diffusion terms.

angular resolution T80 which became operational on 12 August 1987, we decided to use scheme *i* for vertical diffusion and scheme *h* (with adjustment by time filtering under unstable regimes) for the surface processes. The former is both stable, consistent and economical, and the latter has an even larger range of stability.

6. Summary and conclusions

We have discussed a number of time schemes for nonlinear damping equations in atmospheric models, in which the exchange coefficient is a function of static stability. A simple nonlinear damping equation, in which the exchange coefficient is proportional to a power of the dependent variable $C = KX^P$ is analyzed. It is shown that a basic scheme which is frequently used in atmospheric models, in which the exchange coefficient C is computed explicitly (C_n), and the dependent variable implicitly (X_{n+1}), is not only easy to implement, but has a wider range of linear stability than the fully explicit scheme (C_nX_n). The linear stability criterion depends not only on the linear stability parameter $\alpha = C\Delta t$, but also on the power P of the functional relationship between C and X. For strongly nonlinear regimes, the basic scheme *d* becomes linearly unstable, with an amplification factor $\rho < -1$. How-

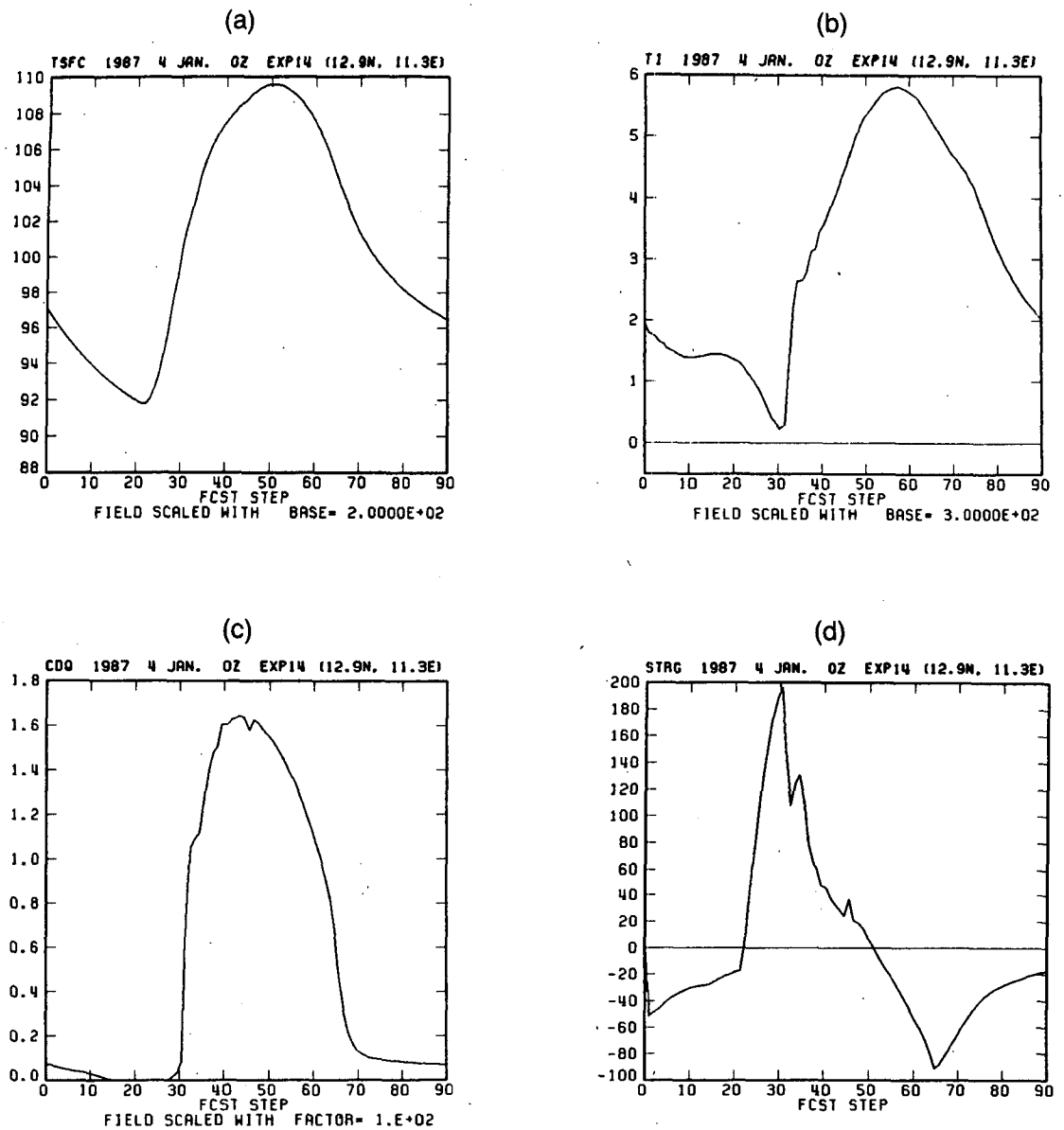

FIG. 8. As in Fig. 7 but with scheme *h* (with the time filter applied for adjustment when the surface layer is unstable) used for the surface processes.

ever, the nonlinear solution remains bounded, oscillating between two values, one much larger than the true solution and one much smaller. It is found that the use of predictor–corrector schemes for the exchange coefficient results in positive (nonoscillatory) amplification factors. For these schemes, however, when the linear stability is violated ($\rho > 1$), the solution is bounded, nonoscillatory but completely wrong. The use of exchange coefficients averaged from time steps n and $n-1$ leads to large amplitude oscillations with a period $3\Delta t$, and therefore is also not recommended. The scheme in which the dependent variable is extrapolated from steps n and $n+1$ $C_n(\gamma X_{n+1} + (1-\gamma)X_n)$ used at ECMWF with $\gamma = 1.5$, is more stable than scheme *d*, and when stable agrees well with centered implicit solutions.

We propose a very simple new scheme, in which the solution is time filtered after scheme *d* is applied:

$$\frac{X_* - X_n}{\Delta t} = -C_n X_*; \quad X_{n+1} = (X_* + X_n)/2.$$

However, since for small Δt this scheme is not consistent (it does not converge to the continuous equation

as $\Delta t \to 0$), we only apply the time filter when scheme *d* is marginally stable or unstable. This scheme has the widest range of linear stability of the schemes considered so far, and requires only a minimal modification of the original scheme *d*. The nonlinear integrations show excellent agreement with the centered implicit method, even in cases in which the other partially explicit schemes fail. In practice, this scheme can be easily implemented by applying the time filter when the atmosphere is neutral or statically unstable, in which case the exchange coefficient changes rapidly from small to large values. An equally simple variant of this scheme:

$$\frac{X_* - X_n}{2\Delta t} = -C_n X_*; \quad \bar{X}_{n+1} = (X_* + X_n)/2,$$

has the advantage of always being consistent, although it has a slightly smaller range of stability.

Numerical experiments with a version of the operational NMC spectral model have led to the choice of the first of the two new schemes presented here for the surface processes, and the second for the vertical diffusion processes. We have also shown that the power P of the nonlinear dependence of the exchange coefficient on temperature can be as large as 3–4 in warm, wet areas under unstable conditions, and even larger when the regime changes from stable to unstable, or vice versa.

Fully implicit schemes are also a possible alternative to solve the problem of the insidious oscillations or wrong nonoscillatory solutions that can appear in atmospheric models when the linear stability of nonlinear damping equations is violated. However, the nonlinearity mentioned above makes them difficult to implement. We have shown that schemes in which the exchange coefficient is computed explicitly (and are therefore easy to implement) and which are combined with a simple time filter under unstable regimes are a good, efficient alternative.

Acknowledgments. We are grateful to M. Jarraud and A. Staniforth for their constructive reviews, to Dr. Pedro Silva-Dias, who pointed out the presence of strong oscillations on the surface temperature of the NMC model over Brazil, and to Dr. David Williamson for reviewing the original manuscript. The experiments of section 4 were performed on a 0.064 MB Commodore computer and a Commodore 1520 printer plotter. The manuscript was typed by Joyce Peters.

APPENDIX

Estimation of the Power *P* of the Exchange Coefficient in the NMC Model

In the simple equation (1.3), we assumed an exchange coefficient of the form $E = KT^P$, and showed that the numerical stability depends not only on the magnitude of E, but also on the power P. In this Appendix we estimate the power P for a more realistic model.

The explicit coefficient, implicit temperature time marching equation of the ground temperature may be written as:

$$\frac{T^{n+1} - T^n}{\Delta t} = -E_s^n(T^{n+1} - T_0) - E_e(q_s^{n+1} - q_0) + R, \quad \text{(A1)}$$

where T is temperature, q specific humidity, q_s the saturation specific humidity corresponding to T and Δt the time increment. The superscript n and subscript 0 stand for time level, and the lowest atmospheric level, respectively. The exchange coefficients E_s and E_e are expressed as:

$$E_s = \rho C_p C_D |V_0| / C$$

$$E_e = \rho L C_D |V_0| \beta / C,$$

where ρ is the density of air, C_p the heat capacity of dry air at constant pressure, C_D is a drag coefficient, $|V_0|$ vector wind magnitude, L the latent heating of condensation, C the heat capacity of the top soil layer, and β the moisture availability.

In order to solve (A1) for T^{n+1}, we use a linear expansion of q_s with respect to temperature, i.e.,

$$\frac{T^{n+1} - T^n}{\Delta t} = -E_s^n(T^{n+1} - T_0) - E_e(q_s^n - q_0) - E_s(T^{n+1} - T^n)\left(\frac{\partial q_s^n}{\partial T}\right). \quad \text{(A2)}$$

Comparing Eq. (A2) and (1.3), the power P of Eq. (1.3) may be estimated by finding the dependency of E_s, E_e, and q_s to the temperature. The E_s and E_e are dependent on T primarily through the C_D, which is determined by solving the similarity function proposed by Businger et al. (1971).

Here, we use a study by Kondo (1975) who estimated a functional form of C_D relating to the stability S:

$$C_D = C_{D0}[0.1 + 0.03S + 0.9\exp(4.8S)] \quad \text{for stable cases}$$

$$C_D = C_{D0}[1 + 0.63S^{1/2}] \quad \text{for unstable cases}$$

where S is proportional to $(T - T_0)$. Here, C_{D0} is the drag coefficient for neutral stratification. Thus the power P is the order of 0.5 or less, but can be much larger when the stratification changes from stable to unstable or vice versa.

The dependency of q_s on the temperature can be estimated from an empirical formula of the polynomial form introduced by Rasmussen (1978). Rough eval-

uation of the polynomial for warmer temperature (considering tropical land areas) indicates that cubic polynomial accounts for up to 90% of the total, indicating the power $P \approx 3$.

The above considerations indicate that the dependence of the exchange coefficient on the temperature over wet, warm areas can correspond to a power as large as $P = 3$–4 within an unstable regime. In addition, when the stratification regime changes from stable to unstable or vice versa, the abrupt changes in the exchange coefficient imply a power even larger (Figs. 5–7). The important effect of this abrupt change, and the high power P that it implies, is underscored by the fact that in the oscillations observed in Fig. 1a, for example, the solution remains trapped in the transition, jumping between the stable and unstable regimes.

REFERENCES

Bidet, Y., B. Bret, G. D'honneur, F. Duvernet, R. Jordan, J. Lepas and S. Planton, 1979: Note technique de L'EERM, no. 6. Projet Amethyste, cahier no. 3. Available from Direction de la Meteorologie 77, rue de Sevres F 92106, Boulogne, Billancourt, France.

Businger, A., J. C. Wyngard, Y. Izumi and E. F. Bradley, 1971: Flux-profile relationships in the atmospheric surface layer. *J. Atmos. Sci.*, **28**, 181–189.

Jarraud, M., A. J. Simmons and M. Kanamitsu, 1985: Development of the high resolution model. ECMWF, Research Dept. Tech. Memo. No. 107, Shinfield Park, Reading, Berkshire, England.

Kondo, J., 1975: Air–sea bulk transfer coefficients in diabatic conditions. *Bound. Layer Meteor.*, **9**, 91–112.

Rasmussen, L. A., 1978: On the approximation of saturation vapor pressure. *J. Appl. Meteor.*, **17**, 1564–1565.

Sela, J., 1988: The New NMC Operational Spectral Model. *Preprints of the AMS Eighth Conf. on Numerical Weather Prediction*, Baltimore, Maryland, 312–313.